THE JOURNAL OF PHYSICAL CHEMISTRY C

Article

Cite This: J. Phys. Chem. C 2019, 123, 9538−9543

pubs.acs.org/JPCC

Comparison Studies of the Linear and Nonlinear Optical Properties of $CsPbBr_xI_{3-x}$ Nanocrystals: The Influence of Dimensionality and Composition

Fuli Zhao,[†,‡,#] Junzi Li,[§,#] Xian Gao,[†] Xin Qiu,[§] Xiaodong Lin,[§] Tingchao He,[*,§] and Rui Chen[*,†]

[†]Department of Electrical and Electronic Engineering, Southern University of Science and Technology, Shenzhen 518055, P. R. China

[‡]College of Arts and Science, Shanghai Dianji University, Shanghai 201306, P. R. China

[§]College of Physics and Optoelectronic Engineering, Shenzhen University, Shenzhen 518060, P. R. China

ABSTRACT: The optoelectronic properties of all-inorganic perovskite nanocrystals (NCs) have been widely investigated, but the relevant studies have mainly focused on $CsPbBr_3$ NCs. The photophysical properties of other all-inorganic perovskite NCs, such as $CsPbBr_xI_{3-x}$ ($0 \le x < 3$), have not been fully explored. Herein, we report comprehensive comparison studies on the linear and nonlinear optical (NLO) properties of colloidal $CsPbBr_xI_{3-x}$ NCs, that is, $CsPbBr_{2.7}I_{0.3}$ two-dimensional nanoplatelets (2D NPs) and cubic NCs of $CsPbBr_{2.7}I_{0.3}$ and $CsPbI_3$. Temperature-dependent photoluminescence (PL) measurements confirm that the 2D NPs exhibit higher PL color purity at elevated temperatures than their cubic counterparts. By using femtosecond-transient absorption spectroscopy, the linear absorption cross sections are determined. Importantly, it is found that the 2D NPs show more efficient volume-normalized two-photon absorption than their cubic counterparts due to the contribution of strong electronic confinement. Studies on the relevant influences of dimensionality and composition on the linear and NLO properties of perovskite NCs are not only interesting for relevant applications but also important for fundamental physics.

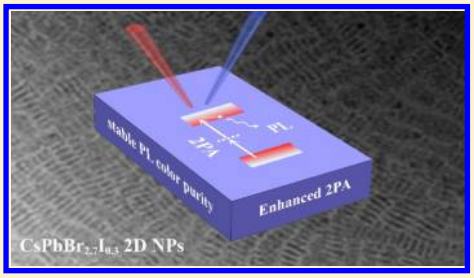

1. INTRODUCTION

Colloidal semiconductor nanocrystals (NCs), currently synthesized with various methods, have been intensively investigated for their various optoelectronic properties.[1,2] Among them, lead halide perovskite NCs and all-inorganic $CsPbX_3$ (X = Cl, Br, I) NCs are emerging as a family of promising light emitters owing to their size- and composition-dependent band gap from the violet to near-infrared region and extremely narrow full width at half-maximum (FWHM).[3−5] The photoluminescence (PL) quantum yields of $CsPbBr_xI_{3-x}$ ($0 \le x < 3$) can reach over 90% in the green and red spectral regions, which enable promising applications as light-emitting diodes and nonlinear optical (NLO) materials.[6−10] Since $CsPbBr_3$ NCs show better stability than $CsPbBr_xI_{3-x}$ NCs, only great progress in the NLO properties of $CsPbBr_3$ NCs has been achieved, while the optical properties of $CsPbBr_xI_{3-x}$ NCs have not been fully elucidated, which significantly hampers their relevant applications.[11,12] Compared with $CsPbBr_3$ NCs, $CsPbBr_xI_{3-x}$ NCs possess some unique properties, mainly (1) longer PL emission wavelengths, (2) longer photoexcited carrier lifetimes and diffusion lengths, and (3) no deep state defects and very small Urbach energy, which are preferable for some special applications, such as solar cells and biological imaging.[13] In addition, the structural stability of $CsPbBr_xI_{3-x}$ NCs has been rapidly improved, supported by efforts in recent studies.[14,15] Therefore, a thorough understanding of their linear and NLO properties is important for the realization of their relevant applications.

It is well known that the NLO properties of semiconductor NCs can be effectively influenced by their geometries. He et al. reported a linear dependence of the three-photon absorption cross section (σ_3) of CdSe NCs on their volume.[16] Xing et al. reported that the σ_3 of CdSe/CdS nanorods follows a superlinear dependence on volume with an exponent of ~1.5.[17] Semiconductor two-dimensional nanoplatelets (2D NPs) offer advantageous optical properties, including narrow PL emission at room temperature together with their large oscillator strength, which can be tuned by their vertical thickness.[2] Due to these favorable features, 2D NPs have become appealing for numerous applications, including NLO devices. For example, Scott et al. found that the magnitudes of the two-photon absorption (2PA) cross sections of CdSe 2D NPs and nanorods are proportional to the square of the volume.[18] The different relationship between the 2PA cross section and volume is attributed to the different degrees of quantum confinement, which is weak for spherical NCs and strong for 2D NPs and nanorods. Although some progress on the geometric influence on the NLO properties of semiconductor NCs has been achieved in recent years, the relevant

Received: January 9, 2019
Revised: February 19, 2019
Published: March 15, 2019

© 2019 American Chemical Society

DOI: 10.1021/acs.jpcc.8b12477
J. Phys. Chem. C 2019, 123, 9538−9543

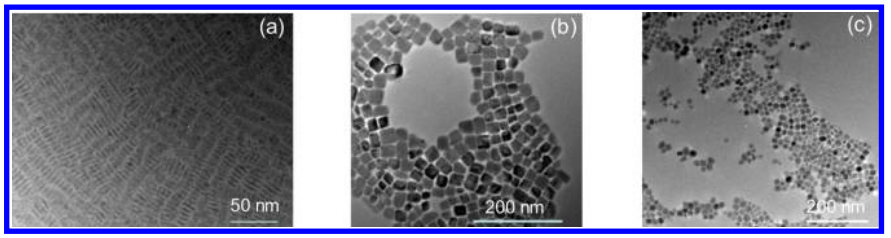

Figure 1. HR-TEM micrographs depicting the atomic resolution of the 2D NPs (a) and cubic NCs of $CsPbBr_{2.7}I_{0.3}$ (b) and $CsPbI_3$ (c).

studies in perovskite NCs have not been well elucidated. It is expected that the strong quantum confinement of perovskite 2D NPs in the vertical direction can greatly improve both their linear optical and NLO properties, which are crucial for high performance in NLO applications.

Herein, we reveal the linear optical and 2PA properties of $CsPbBr_{2.7}I_{0.3}$ 2D NPs and cubic NCs of $CsPbBr_{2.7}I_{0.3}$ and $CsPbI_3$. Compared with the cubic counterparts, the $CsPbBr_{2.7}I_{0.3}$ 2D NPs possess better PL color purity at elevated temperatures. Importantly, $CsPbBr_{2.7}I_{0.3}$ 2D NPs exhibit enhanced volume-normalized (NV) 2PA properties over the wavelength range of 720−880 nm, which will enable new approaches for various applications.

2. EXPERIMENTAL SECTION

2.1. Sample Preparation. Cubic NCs of $CsPbBr_{2.7}I_{0.3}$ and $CsPbI_3$ were prepared according to the previously published method described in ref 2 with slight modifications. Additionally, $CsPbBr_{2.7}I_{0.3}$ NPs were synthesized according to the procedures provided in ref 19.

2.2. TEM and Steady-State Spectroscopy. The morphology and size distribution of the NCs were examined using transmission electron microscopy (TEM; JEOL, JEM-2010). Linear absorption measurements were carried out using a UV−vis−NIR spectrophotometer (Lambda 950, PerkinElmer, Inc.). The one-photon PL spectra and absolute quantum yields were collected with a spectrometer (Zolix, SENS-9000).

2.3. Lifetime Measurements. Time-resolved PL experiments were carried out at room temperature. The excitation source was a pulsed ultraviolet picosecond diode laser operating at 375 nm, and the pulse width and repetition rate of the laser were 80 ps and 50 MHz, respectively. The signal was dispersed by a 320 mm monochromator (iHR320 from Horiba, Ltd.) combined with suitable filters and detected by a time-correlated single photon counting technique.

2.4. Measurements of Temperature-Dependent PL Spectra. The PL measurements were performed between 10 and 300 K within a closed-cycle helium cryostat. A CW He−Cd laser emitting at 325 nm was used as the PL excitation source, and the signal was dispersed by a 750 mm monochromator combined with suitable filters and detected by a photomultiplier by using a standard lock-in amplifier technique.

2.5. Measurements of Femtosecond-Transient Absorption (fs-TA) Spectrum. The fs-TA spectra and dynamics were recorded using a standard pump−probe configuration at 350 nm, ∼100 fs pump pulses at a 1 kHz repetition rate, and a broad-band white-light supercontinuum probe (18SI80466 Rev.1, Newport). The excited spot diameter was 300 μm, and the measured quantity was the normalized transmission change, that is, $\Delta A/A$, which was performed on NC solutions with an optical density below 1 at the excitation wavelength.

2.6. Measurements of Two-Photon Excited PL Spectra and 2PA Cross Sections. Room-temperature two-photon excited PL spectra of the perovskite NCs were also measured with laser pulses (1000 Hz, 100 fs) from an optical parameter amplifier combined with a traveling-wave optical parameter amplifier system (TOPAS, Spectra-Physics, Inc.) with a tunable wavelength range. The emission from the samples was collected at a backscattering angle into an optical fiber that was coupled to a spectrometer (Acton, SpectraPro 2500i). The 2PA cross sections of perovskite NCs in toluene solution were investigated via the standard Z-scan technique[20] with the same excitation source as that used in the measurements of the two-photon excited PL.

3. RESULTS AND DISCUSSION

As shown in Figure 1, $CsPbBr_{2.7}I_{0.3}$ 2D NPs were crystallized with lateral sizes of 16 and 26 nm. The majority of the 2D NPs had a thickness of ∼2.4 nm, which corresponds to four unit cells. The as-formed colloidal NCs of $CsPbBr_{2.7}I_{0.3}$ and $CsPbI_3$ were ∼19 and ∼15 nm in size with nearly cubic shapes, respectively. The volumes were calculated as ∼998, ∼6859, and ∼3375 nm^3 for the 2D NPs and cubic NCs of $CsPbBr_{2.7}I_{0.3}$ and $CsPbI_3$, respectively. The UV−vis absorption and PL spectra of the perovskite NCs were measured (Figure 2a). For the 2D NPs, a clear excitonic absorption peak can be observed at 459 nm, while the other two samples do not exhibit such peaks. All three samples show bright PL emission (inset of Figure 2a), and each PL spectrum clearly comprises only a single narrow peak, with the central peak positions at 471, 550,

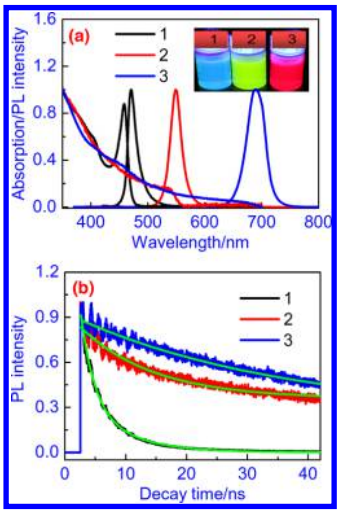

Figure 2. (a) UV−vis absorption and PL spectra of the perovskite NCs. The inset shows their colloidal solutions under UV illumination (λ = 365 nm). (b) Time-resolved fluorescence decay curves of the perovskite NCs. 1, 2, and 3 represent 2D NPs and cubic NCs of $CsPbBr_{2.7}I_{0.3}$ and $CsPbI_3$, respectively.

DOI: 10.1021/acs.jpcc.8b12477
J. Phys. Chem. C 2019, 123, 9538−9543

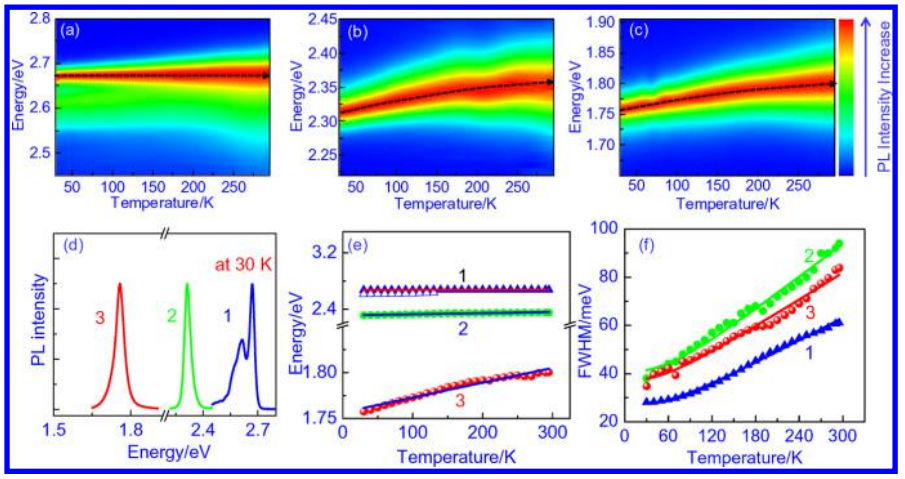

Figure 3. Temperature-dependent PL spectra of the 2D NPs (a) and cubic NCs of $CsPbBr_{2.7}I_{0.3}$ (b) and $CsPbI_3$ (c). The solid lines are guide for the eye. (d) PL spectra of the NCs at 30 K. (e) Temperature-dependent NC band gap derived from the center emission wavelength. The solid lines represent Varshni fits of the data. (f) Temperature-dependent PL linewidths of the perovskite NCs. The solid lines are the fits obtained using a model for thermal broadening. (d–f) 1, 2, and 3 represent the 2D NPs and cubic NCs of $CsPbBr_{2.7}I_{0.3}$ and $CsPbI_3$, respectively.

and 691 nm for the 2D NPs and cubic NCs of $CsPbBr_{2.7}I_{0.3}$ and $CsPbI_3$, respectively. The absolute PL quantum yields of $CsPbBr_{2.7}I_{0.3}$ 2D NPs and cubic NCs of $CsPbBr_{2.7}I_{0.3}$ and $CsPbI_3$ were determined to be 4.5, 9.5, and 15.1%, respectively. In addition, the determination of lifetime values of semiconductor NCs is important for many applications, such as various nonlinear photonic devices and two-photon lifetime bioimaging. In the latter case, the signals from short-lived autofluorescence can be greatly reduced if the semiconductor NCs with long lifetime are used.[21] Time-resolved fluorescence decay curves of the NCs were then measured (Figure 2b). By fitting with a single exponential or biexponential function, we obtained average radiative lifetime values of 3.2, 10.1, and 12.2 ns, respectively. The much shorter lifetime of the 2D NPs is generally considered to be due to a high density of structural defects and trap states.[22] Additionally, the lifetime values of all-inorganic perovskite NCs are much smaller than those of hybrid inorganic–organic perovskite NCs.[23] Actually, the nature of the longer lifetime of hybrid inorganic–organic perovskite NCs is unclear and often argued. Several microscopic mechanisms have been proposed to interpret their long lifetime, such as formation of large polarons, Rashba effect, ferroelectric domains, photon recycling, and the screening of band-edge charge carriers by rotation of organic cation molecules.[24] However, recent work demonstrated that the screening effect was nonessential.[25]

Since understanding the interactions between carriers and lattice vibrations (phonons) is a prerequisite for the fabrication of nonlinear optoelectronic devices, the exciton–phonon interactions of perovskite NCs should be investigated. Although such properties of other perovskite NCs have been widely reported,[26−28] the relevant studies on our materials have not been revealed. To shed more light on the exciton–phonon interactions of NCs, we conducted temperature-dependent PL measurements for thin films of perovskite NCs obtained by a drop-casting method. Pseudocolor maps of the temperature-dependent PL spectra of perovskite NCs with different geometries in the temperature range of 30 to 300 K are presented in Figure 3a–c. A double-peak PL spectrum was observed for $CsPbBr_{2.7}I_{0.3}$ 2D NPs but not for the other two samples (Figure 3d). The PL at low energy is attributed to emission from bound excitons, which are trapped at shallow energy defects before recombination, while the PL at high energy results from free excitons.[29] Compared with their cubic counterparts, 2D NPs have appreciable defect states that produce PL emission from bound excitons. It can be seen that the PL peaks of the NCs were continuously blue-shifted with the increase in temperature from 30 to 300 K (Figure 3e). Thermal changes in the band gap were fitted using the empirical Varshni relation as follows

$$E(T) = E(0) - \frac{\alpha T^2}{\beta + T} \tag{1}$$

where $E(T)$ and $E(0)$ are the band gaps at temperature T and 0 K, respectively, α is the coefficient of the band gap change, and β is the Debye temperature for the material.[30] The values of α were determined to be -2.1×10^{-5} K^{-2} for the 2D NPs and -1.5×10^{-4} and -1.6×10^{-4} K^{-2} for the cubic NCs of $CsPbBr_{2.7}I_{0.3}$ and $CsPbI_3$, respectively. The thermal change in the band gaps of the cubic NCs of $CsPbBr_{2.7}I_{0.3}$ and $CsPbI_3$ is 1 order of magnitude larger than that of $CsPbBr_{2.7}I_{0.3}$ 2D NPs, indicating their high PL color purity at elevated temperatures. The strong quantum confinement in the 2D NPs can greatly enhance their exciton binding energy (E_b).[31] The higher E_b value indicates that the excitons are highly stable and the probability for their dissociation is less, in particular at temperatures T < 300 K. As a result, the thermal change in the band gap of 2D NPs was much smaller than that of the cubic NCs of $CsPbBr_{2.7}I_{0.3}$ and $CsPbI_3$. The thermal broadening of the excitonic peak is generally interpreted as an exciton–phonon interaction. The temperature dependence of the PL FWHM can be approximately described by the following equation:

$$\Gamma(T) = \Gamma_0 + \Gamma_{ac} + \Gamma_{LO} = \Gamma_0 + \gamma_{ac}T + \gamma_{LO}N_{LO}(T)$$
$$= \Gamma_0 + \gamma_{ac}T + \frac{\gamma_{LO}}{e^{E_{LO}/k_BT} - 1} \tag{2}$$

In eq 2, Γ_0 is the inhomogeneous peak width at 0 K, while Γ_{ac} and Γ_{LO} are homogeneous PL emission broadening terms, which result from acoustic and longitudinal optical (LO) phonon scattering, respectively. The coefficients γ_{ac} and γ_{LO} represent the weights of the exciton–phonon coupling strengths. $N_{LO}(T)$ describes the occupation numbers of the

DOI: 10.1021/acs.jpcc.8b12477
J. Phys. Chem. C 2019, 123, 9538−9543

respective LO phonons, and E_{LO} is the phonon energy involved in LO phonon scattering.[32] Figure 3f shows the temperature dependence of the PL FWHM of the free excitons of the perovskite NCs. The solid lines represent the fitting results based on eq 2. The best-fitted values of γ_{LO} for the 2D NPs and cubic NCs of $CsPbBr_{2.7}I_{0.3}$ and $CsPbI_3$ are 38, 32, and 31 meV, and the values of E_{LO} were determined to be 14.9, 20, and 14.2 meV, respectively.

Then, we estimated the linear absorption cross sections (σ_{lin}) of the perovskite NCs from the excitation intensity-dependent one-photon-induced ground state bleaching (GSB) signals via fs-TA spectroscopy.[33] As shown in Figure 4a, we

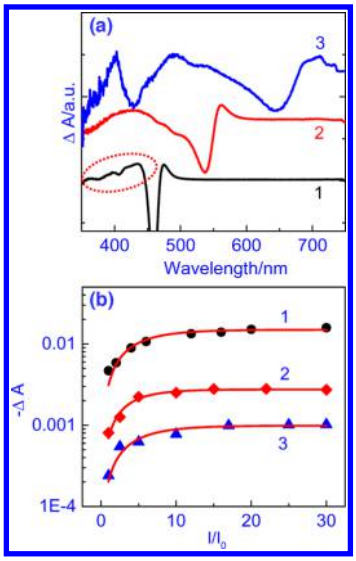

Figure 4. (a) fs-TA data for the perovskite NCs at 4 ps under excitation at 350 nm. The curve circled by the dashed lines indicates a multimodal feature. (b) Excitation intensity-dependent GSB signal amplitude at a time delay of 1 ns for the perovskite NCs. The solid curves are theoretical fits. 1, 2, and 3 represent the 2D NPs and cubic NCs of $CsPbBr_{2.7}I_{0.3}$ and $CsPbI_3$, respectively.

present the fs-TA spectra of the perovskite NCs excited by pump pulses at 350 nm. For all perovskite NCs, the fs-TA spectra exhibit two broad positive bands spanning the visible region and a broad negative band. The broad negative band is attributed to the superposition of GSB and simulated emission due to the close resemblance to the spectra of steady absorption and PL, while the positive spectral features are assigned to photoinduced absorption of the excited state.[34] It was found that the photoinduced absorption feature develops a multimodal feature for the 2D NPs, indicating the strong confinement regime. However, such a feature has not been observed in the cubic NCs of $CsPbBr_{2.7}I_{0.3}$ and $CsPbI_3$, suggesting weak quantum confinement. The different features can be understood in terms of the different confinement regimes defined based on the NC dimensions relative to the exciton Bohr radius. After fast Auger recombination within the initial hundreds of picoseconds, the samples contain only a single exciton in the subsequent time period. The amplitude of the GSB signal under different excitation intensities varies based on the following equation

$$-A(I/I_0) = -A_{max}[1 - e^{-(I/I_0)\sigma_{lin}I_0}] \quad (3)$$

where $A(I/I_0)$ denotes the GSB signal amplitude of the NCs after a long time delay as a function of excitation intensity and I_0 is the minimum excitation intensity used in the fs-TA experiment.[33] As shown in Figure 4b, the excitation intensity-dependent GSB signal amplitude with a delay time of 1 ns could be well fitted with eq 3, from which the values of σ_{lin} at 350 nm were extracted and determined to be $\sim 7.4 \times 10^{-14}$, $\sim 9.7 \times 10^{-14}$, and $\sim 6.2 \times 10^{-14}$ cm^2 for the 2D NPs and cubic NCs of $CsPbBr_{2.7}I_{0.3}$ and $CsPbI_3$, respectively. Their NV linear absorption cross sections were calculated to be $\sim 7.4 \times 10^{-17}$, $\sim 1.4 \times 10^{-17}$, and $\sim 1.8 \times 10^{-17}$ cm^2/nm^3, respectively. The largest NV linear absorption cross section of 2D NPs is due to their strongest quantum confinement effect. Correspondingly, their molar distinction coefficients were determined to be $\sim 1.93 \times 10^7$, $\sim 2.54 \times 10^7$, and $\sim 1.63 \times 10^7$ $L \cdot cm^{-1} \cdot mol^{-1}$ at 350 nm.

From Figure 2a, one can also see that there is one spectral window for the perovskite NCs with negligible one-photon absorption, that is, from ~700 to ~900 nm, which is suitable for two-photon excitation. The 2PA mechanism can be confirmed by measurements of the power-dependent PL intensity (inset of Figure 5a). The logarithm−logarithm plot of

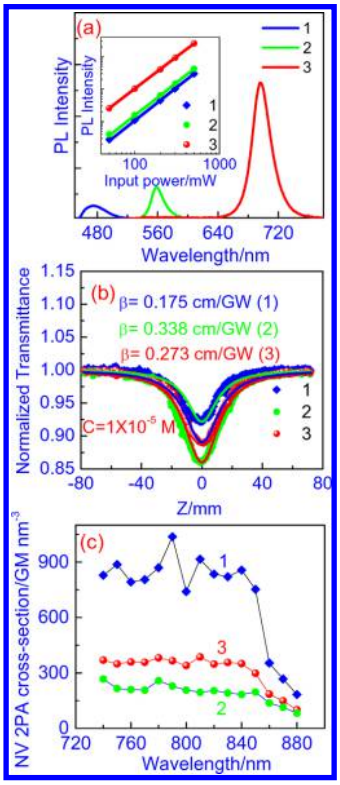

Figure 5. (a) PL spectra of the perovskite NCs recorded under excitation at 800 nm. The inset shows the quadratic dependence of the PL emission intensity on the input power. (b) Typical open aperture Z-scan curves at 800 nm. The solid lines are the theoretical fitted data. (c) Comparison of the NV 2PA cross sections of different perovskite NCs. 1, 2, and 3 represent the 2D NPs and cubic NCs of $CsPbBr_{2.7}I_{0.3}$ and $CsPbI_3$, respectively.

the quadratic dependence of the PL intensity versus pumping power with a slope of approximately 2 clearly confirms the existence of the 2PA process.[35] To quantitatively determine the 2PA cross sections of the 2D NPs and cubic NCs, Z-scan measurements were carried out and relevant experimental data are presented in Figure 5b. To understand the influence of quantum confinement on the 2PA properties, comparing the

DOI: 10.1021/acs.jpcc.8b12477
J. Phys. Chem. C 2019, 123, 9538−9543

2PA cross section at a single excitation wavelength is less than ideal because it does not account for the spectral dependence of the 2PA. Thus, we measured the 2PA spectra of the perovskite NCs in the spectral region between 720 and 880 nm. Since the volume of the NCs greatly influence the 2PA but does not alter the spectral course, we plot the NV 2PA cross section (in GM/nm^3) rather than the absolute cross section (Figure 5c).[8,36] For all samples, the NV 2PA values increase when the excitation wavelength is tuned from low to high energies. Additionally, they all show nearly constant NV 2PA cross sections for excitation wavelengths between 740 and 850 nm. The reason that the 2PA spectra do not follow the spectral behavior of linear absorption is possibly due to the distinct selection rules and influence of scattering at higher excitation energies.[37] The NV 2PA cross sections of the perovskite NCs show a very strong geometry dependence. Specifically, the maximum NV σ_2 value of the $CsPbBr_{2.7}I_{0.3}$ 2D NPs is 346 GM/nm^3, which is 4.0 and 2.7 times larger than those of $CsPbBr_{2.7}I_{0.3}$ (~86 GM/nm^3) and $CsPbI_3$ cubic NCs (~127 GM/nm^3). In addition, it was several times smaller than that of $CsPbBr_3$ 2D NPs and was comparable with those of $CsPbBr_3$ cubic NCs.[8] However, the NV 2PA cross sections of 2D NPs are 1−2 orders of magnitude larger than those of the cubic NCs of $CsPbCl_3$ and $CsPb(Cl_{0.53}Br_{0.47})_3$,[38] spherical CdTe NCs,[39] and organic dots.[40] Additionally, it was found that the NV 2PA cross sections of $CsPbBr_{2.7}I_{0.3}$ and $CsPbI_3$ cubic NCs were 1 order of magnitude larger than those of $CsPbCl_3$ and $CsPb(Cl_{0.53}Br_{0.47})_3$ cubic NCs,[30] indicating that the addition of Br and I elements can more effectively amplify the 2PA of perovskite NCs compared with the addition of the Cl element. However, the 2PA cross section of the perovskite NCs can only be slightly modified by partially changing the halide element from Br to I. Thus, compared with the change in the halide element in their cubic counterparts, the fabrication of $CsPbBr_xI_{3-x}$ NCs with a 2D geometry can more efficiently amplify the 2PA cross sections. It can be concluded that the electronic confinement effects could also result in very high NV 2PA cross sections for $CsPbI_3$ 2D NPs if their poor stability could be overcome.

4. CONCLUSIONS

In conclusion, our findings reveal that a family of halide perovskite colloidal NCs, that is, 2D NPs and cubic NCs of $CsPbBr_{2.7}I_{0.3}$ and $CsPbI_3$ cubic NCs, possesses dramatically different linear and NLO properties. Compared with their cubic counterparts, the 2D NPs of $CsPbBr_{2.7}I_{0.3}$ exhibit higher PL color purity but more dramatic FWHM broadening at elevated temperatures. Importantly, the perovskite NCs with a 2D geometry offer amazing NV 2PA cross sections that are much larger than those of their cubic counterparts, highlighting their potential for nonlinear optics and bioimaging applications.

AUTHOR INFORMATION

Corresponding Authors

*E-mail: tche@szu.edu.cn (T.H.).
*E-mail: chenr@sustech.edu.cn (R.C.).

ORCID

Rui Chen: 0000-0002-0445-7847

Author Contributions

#F.Z. and J.L. contributed equally to this work.

Notes

The authors declare no competing financial interest.

ACKNOWLEDGMENTS

We thank the National Natural Science Foundation of China (No. 11574130) and the Shenzhen Science and Technology Innovation Commission (Nos.: JCYJ20170302142433007, KQJSCX20170726145748464, and KQTD2015071710313656). R.C. acknowledges support from the National 1000 Plan for Young Talents.

REFERENCES

(1) Wang, Y.; Ta, V. D.; Leck, K. S.; Tan, B. H. I.; Wang, Z.; He, T.; Ohl, C.-D.; Demir, H. V.; Sun, H. Robust Whispering-Gallery-Mode Microbubble Lasers from Colloidal Quantum Dots. *Nano Lett.* **2017**, *17*, 2640−2646.

(2) Akkerman, Q. A.; Motti, S. G.; Srimath Kandada, A. R.; Mosconi, E.; D'Innocenzo, V.; Bertoni, G.; Marras, S.; Kamino, B. A.; Miranda, L.; De Angelis, F.; et al. Solution Synthesis Approach to Colloidal Cesium Lead Halide Perovskite Nanoplatelets with Monolayer-Level Thickness Control. *J. Am. Chem. Soc.* **2016**, *138*, 1010−1016.

(3) Huang, H.; Bodnarchuk, M. I.; Kershaw, S. V.; Kovalenko, M. V.; Rogach, A. L. Lead Halide Perovskite Nanocrystals in the Research Spotlight: Stability and Defect Tolerance. *ACS Energy Lett.* **2017**, *2*, 2071−2083.

(4) Parobek, D.; Roman, B. J.; Dong, Y.; Jin, H.; Lee, E.; Sheldon, M.; Son, D. H. Exciton-to-Dopant Energy Transfer in Mn-Doped Cesium Lead Halide Perovskite Nanocrystals. *Nano Lett.* **2016**, *16*, 7376−7380.

(5) Protesescu, L.; Yakunin, S.; Bodnarchuk, M. I.; Krieg, F.; Caputo, R.; Hendon, C. H.; Yang, R. X.; Walsh, A.; Kovalenko, M. V. Nanocrystals of Cesium Lead Halide Perovskites ($CsPbX_3$, X = Cl, Br, and I): Novel Optoelectronic Materials Showing Bright Emission with Wide Color Gamut. *Nano Lett.* **2015**, *15*, 3692−3696.

(6) Wang, Y.; Li, X.; Zhao, X.; Xiao, L.; Zeng, H.; Sun, H. Nonlinear Absorption and Low-Threshold Multiphoton Pumped Stimulated Emission from All-Inorganic Perovskite Nanocrystals. *Nano Lett.* **2016**, *16*, 448−453.

(7) He, T.; Li, J.; Qiu, X.; Xiao, S.; Lin, X. Superior Multiphoton Absorption Properties in Colloidal Mn-Doped $CsPbCl_3$ Two-Dimensional Nanoplatelets. *Photonics Res.* **2018**, *6*, 1021−1027.

(8) He, T.; Li, J.; Qiu, X.; Xiao, S.; Yin, C.; Lin, X. Highly Enhanced Normalized-Volume Multiphoton Absorption in $CsPbBr_3$ 2D Nanoplates. *Adv. Opt. Mater.* **2018**, *6*, 1800843.

(9) Chen, W.; Bhaumik, S.; Veldhuis, S. A.; Xing, G.; Xu, Q.; Grätzel, M.; Mhaisalkar, S.; Mathews, N.; Sum, T. C. Giant Five-Photon Absorption from Multidimensional Core-Shell Halide Perovskite Colloidal Nanocrystals. *Nat. Commun.* **2017**, *8*, 15198.

(10) Chen, J.; Chábera, P.; Pascher, T.; Messing, M. E.; Schaller, R.; Canton, S.; Zheng, K.; Pullerits, T. Enhanced Size Selection in Two-Photon Excitation for $CsPbBr_3$ Perovskite Nanocrystals. *J. Phys. Chem. Lett.* **2017**, *8*, 5119−5124.

(11) Zheng, Z.; Wang, X.; Shen, Y.; Luo, Z.; Li, L.; Gan, L.; Ma, Y.; Li, H.; Pan, A.; Zhai, T. Space-Confined Synthesis of 2D All-Inorganic $CsPbI_3$ Perovskite Nanosheets for Multiphoton-Pumped Lasing. *Adv. Opt. Mater.* **2018**, *6*, 1800879.

(12) Liu, S.; Chen, G.; Huang, Y.; Lin, S.; Zhang, Y.; He, M.; Xiang, W.; Liang, X. Tunable Fluorescence and Optical Nonlinearities of All Inorganic Colloidal Cesium Lead Halide Perovskite Nanocrystals. *J. Alloys Compd.* **2017**, *724*, 889−896.

(13) Shen, Q.; Ripolles, T. S.; Even, J.; Ogomi, Y.; Nishinaka, K.; Izuishi, T.; Nakazawa, N.; Zhang, Y.; Ding, C.; Liu, F.; et al. Slow Hot Carrier Cooling in Cesium Lead Iodide Perovskites. *Appl. Phys. Lett.* **2017**, *111*, 153903.

(14) Dutta, A.; Dutta, S. K.; Das Adhikari, S.; Pradhan, N. Phase-Stable $CsPbI_3$ Nanocrystals: The Reaction Temperature Matters. *Angew. Chem. Int. Ed.* **2018**, *57*, 9083−9087.

DOI: 10.1021/acs.jpcc.8b12477
J. Phys. Chem. C 2019, 123, 9538−9543

(15) Liu, Y.; Li, F.; Liu, Q.; Xia, Z. Synergetic Effect of Postsynthetic Water Treatment on the Enhanced Photoluminescence and Stability of $CsPbX_3$ (X = Cl, Br, I) Perovskite Nanocrystals. *Chem. Mater.* **2018**, *30*, 6922−6929.
(16) He, G. S.; Yong, K.-T.; Zheng, Q.; Sahoo, Y.; Baev, A.; Ryasnyanskiy, A. I.; Prasad, P. N. Multi-Photon Excitation Properties of CdSe Quantum Dots Solutions and Optical Limiting Behavior in Infrared Range. *Opt. Express* **2007**, *15*, 12818−12833.
(17) Xing, G.; Chakrabortty, S.; Ngiam, S. W.; Chan, Y.; Sum, T. C. Three-Photon Absorption in Seeded CdSe/CdS Nanorod Heterostructures. *J. Phys. Chem. C* **2011**, *115*, 17711−17716.
(18) Scott, R.; Achtstein, A. W.; Prudnikau, A.; Antanovich, A.; Christodoulou, S.; Moreels, I.; Artemyev, M.; Woggon, U. Two Photon Absorption in II−VI Semiconductors: The Influence of Dimensionality and Size. *Nano Lett.* **2015**, *15*, 4985−4992.
(19) Liang, Z.; Zhao, S.; Xu, Z.; Qiao, B.; Song, P.; Gao, D.; Xu, X. Shape-Controlled Synthesis of All-Inorganic $CsPbBr_3$ Perovskite Nanocrystals with Bright Blue Emission. *ACS Appl. Mater. Interfaces* **2016**, *8*, 28824−28830.
(20) Sheik-Bahae, M.; Said, A. A.; Wei, T.-H.; Hagan, D. J.; Van Stryland, E. W. Sensitive Measurement of Optical Nonlinearities Using a Single Beam. *IEEE J. Quantum Electron.* **1990**, *26*, 760−769.
(21) He, T.; Ren, C.; Li, Z.; Xiao, S.; Li, J.; Lin, X.; Ye, C.; Zhang, J.; Guo, L.; Hu, W.; et al. Thermally Activated Delayed Fluorescence Organic Dots for Two-Photon Fluorescence Lifetime Imaging. *Appl. Phys. Lett.* **2018**, *112*, 211102.
(22) Bohn, B. J.; Tong, Y.; Gramlich, M.; Lai, M. L.; Döblinger, M.; Wang, K.; Hoye, R. L. Z.; Müller-Buschbaum, P.; Stranks, S. D.; Urban, A. S.; et al. Boosting Tunable Blue Luminescence of Halide Perovskite Nanoplatelets through Postsynthetic Surface Trap Repair. *Nano Lett.* **2018**, *18*, 5231−5238.
(23) Levchuk, I.; Osvet, A.; Tang, X.; Brandl, M.; Perea, J. D.; Hoegl, F.; Matt, G. J.; Hock, R.; Batentschuk, M.; Brabec, C. J. Brightly Luminescent and Color-Tunable Formamidinium Lead Halide Perovskite $FAPbX_3$ (X = Cl, Br, I) Colloidal Nanocrystals. *Nano Lett.* **2017**, *17*, 2765−2770.
(24) Chen, T.; Chen, W.-L.; Foley, B. J.; Lee, J.; Ruff, J. P. C.; Ko, J. Y. P.; Brown, C. M.; Harriger, L. W.; Zhang, D.; Park, C.; Yoon, M.; et al. Origin of Long Lifetime of Band-Edge Charge Carriers in Organic−Inorganic Lead Iodide Perovskites. *Proc. Natl. Acad. Sci. U. S. A.* **2017**, *114*, 7519−7524.
(25) Dastidar, S.; Li, S.; Smolin, S. Y.; Baxter, J. B.; Fafarman, A. T. Slow Electron−Hole Recombination in Lead Iodide Perovskites Does Not Require a Molecular Dipole. *ACS Energy Lett.* **2017**, *2*, 2239−2244.
(26) Diroll, B. T.; Zhou, H.; Schaller, R. D. Low-Temperature Absorption, Photoluminescence, and Lifetime of $CsPbX_3$ (X = Cl, Br, I) Nanocrystals. *Adv. Funct. Mater.* **2018**, *28*, 1800945.
(27) Diroll, B. T.; Nedelcu, G.; Kovalenko, M. V.; Schaller, R. D. High-Temperature Photoluminescence of $CsPbX_3$ (X = Cl, Br, I) Nanocrystals. *Adv. Funct. Mater.* **2017**, *27*, 1606750.
(28) Ghosh, S.; Shi, Q.; Pradhan, B.; Kumar, P.; Wang, Z.; Acharya, S.; Pal, S. K.; Pullerits, T.; Karki, K. J. Phonon Coupling with Excitons and Free Carriers in Formamidinium Lead Bromide Perovskite Nanocrystals. *J. Phys. Chem. Lett.* **2018**, *9*, 4245−4250.
(29) Woo, H. C.; Choi, J. W.; Shin, J.; Chin, S.-H.; Ann, M. H.; Lee, C.-L. Temperature-Dependent Photoluminescence of $CH_3NH_3PbBr_3$ Perovskite Quantum Dots and Bulk Counterparts. *J. Phys. Chem. Lett.* **2018**, *9*, 4066−4074.
(30) Varshni, Y. P. Temperature Dependence of the Energy Gap in Semiconductors. *Physica* **1967**, *34*, 149−154.
(31) Hintermayr, V. A.; Polavarapu, L.; Urban, A. S.; Feldmann, J. Accelerated Carrier Relaxation through Reduced Coulomb Screening in Two-Dimensional Halide Perovskite Nanoplatelets. *ACS Nano* **2018**, *12*, 10151−10158.
(32) Viswanath, A. K.; Lee, J. I.; Kim, D.; Lee, C. R.; Leem, J. Y. Exciton-Phonon Interactions, Exciton Binding Energy, and Their Importance in the Realization of Room-Temperature Semiconductor Lasers Based on GaN. *Phys. Rev. B* **1998**, *58*, 16333.
(33) Chen, J.; Žídek, K.; Chábera, P.; Liu, D.; Cheng, P.; Nuuttila, L.; Al-Marri, M. J.; Lehtivuori, H.; Messing, M. E.; Han, K.; Zheng, K.; Pullerits, T. Size- and Wavelength-Dependent Two-Photon Absorption Cross-Section of $CsPbBr_3$ Perovskite Quantum Dots. *J. Phys. Chem. Lett.* **2017**, *8*, 2316−2321.
(34) Butkus, J.; Vashishtha, P.; Chen, K.; Gallaher, J. K.; Prasad, S. K. K.; Metin, D. Z.; Laufersky, G.; Gaston, N.; Halpert, J. E.; Hodgkiss, J. M. The Evolution of Quantum Confinement in CsPbBr3 Perovskite Nanocrystals. *Chem. Mater.* **2017**, *29*, 3644−3652.
(35) He, G. S.; Tan, L. S.; Zheng, Q.; Prasad, P. N. Multiphoton Absorbing Materials: Molecular Designs, Characterizations, and Applications. *Chem. Rev.* **2008**, *108*, 1245−1330.
(36) Padilha, L. A.; Nootz, G.; Olszak, P. D.; Webster, S.; Hagan, D. J.; Van Stryland, E. W.; Levina, L.; Sukhovatkin, V.; Brzozowski, L.; Sargent, E. H. Optimization of Band Structure and Quantum-Size-Effect Tuning for Two-Photon Absorption Enhancement in Quantum Dots. *Nano Lett.* **2011**, *11*, 1227−1231.
(37) Nagamine, G.; Rocha, J. O.; Bonato, L. G.; Nogueira, A. F.; Zaharieva, Z.; Watt, A. A. R.; de Brito Cruz, C. H.; Padilha, L. A. Two-Photon Absorption and Two-Photon-Induced Gain in Perovskite Quantum Dots. *J. Phys. Chem. Lett.* **2018**, *9*, 3478−3484.
(38) Li, J.; Ren, C.; Qiu, X.; Lin, X.; Chen, R.; Yin, C.; He, T. Ultrafast Optical Nonlinearity of Blue-Emitting Perovskite Nanocrystals. *Photonics Res.* **2018**, *6*, 554−559.
(39) Pu, S. C.; Yang, M. J.; Hsu, C. C.; Lai, C. W.; Hsieh, C. C.; Lin, S. H.; Cheng, Y. M.; Chou, P. T. The Empirical Correlation between Size and Two-Photon Absorption Cross Section of CdSe and CdTe Quantum Dots. *Small* **2006**, *2*, 1308−1313.
(40) He, T.; Hu, W.; Shi, H.; Pan, Q.; Ma, G.; Huang, W.; Fan, Q.; Lin, X. Strong Nonlinear Optical Phosphorescence from Water-Soluble Polymer Dots: Towards the Application of Two-Photon Bioimaging. *Dyes Pigm.* **2015**, *123*, 218−221.

DOI: 10.1021/acs.jpcc.8b12477
J. Phys. Chem. C 2019, 123, 9538−9543